Simulation and Performance of a Cosmic Ray Fluorescence Detector

Ronald C. Shellard*, Johana C. Diaz†
Centro Brasileiro de Pesquisas Físicas
Rua Dr. Xavier Sigaud 150,
Rio de Janeiro,22290-180, RJ, Brasil

Marcia G. do Amaral‡
Instituto de Física, Universidade Federal Fluminense
Av. Litorânea s/n, Campus da Praia Vermelha,
Niterói, CEP 24210-340, RJ, Brazil

Recebido em 10 de abril, 2000. Aceito em 08 de novembro de 2000.

We study the performance and the efficiency of Fluorescence Detectors used in the investigation of cosmic ray showers of very high energy. This study is based on a simulation of the performance of the Pierre Auger Observatory in the Pampa Amarilla site, for cosmic rays with primary energies ranging from 10^{18} eV to 10^{21} eV. We analyze the effects in the efficiency of changing triggering conditions in single and stereo mode events.

Estudamos a performance e a eficiência dos Detectores de Fluorescência usados na investigação de chuveiros atmosféricos intensos ultra-energéticos. Este trabalho se baseia nos resultados de uma simulação da performance do Observatório Pierre Auger no sítio de Pampa Amarilla para raios cósmicos com energias primárias que variam desde 10^{18} eV até 10^{21} eV. Analisamos os efeitos sobre a eficiência obtida ao variarmos as condições de seleção do "trigger" nos modos "single" e "stereo".

I Introduction

Since cosmic rays were first observed in 1912 by the Austrian physicist Victor Hess, all the efforts made by the cosmic rays physics community all around the world were concentrated in the determination of their primary composition, their source and spectrum. Pierre Auger gave an important contribution to the study of cosmic ray physics when he measured the correlation of cosmic rays at the scale of ten's of meters and inferred, correctly, their association in extensive air showers (EAS) and that their spectrum could go beyond 10^{15} eV [1]. Cosmic Rays with energies beyond 10^{19} eV were first detected by Linsley [2], with the Volcano Ranch Array, in the beginning of the 60's. Since then, many other groups have reported results on the detection of similar type of extremely high energy cosmic rays (EHE)[3][4][5] [6][7]. In spite of the extensive research and the impressive amount of data collected in the detection of these events, very much is still unknown about the nature and origin of those EHE cosmic rays, once the data is not enough to ensure the detailed characterization of them. The reason for this is that, at these high energies, the flux is very low (the rate of cosmic rays above 10^{20} eV is one event/km^2/century), so that in order to obtain a reasonable rate of events, very large detectors with huge acceptances are required. The current projects in operation, like the Fly's Eye HiRes[16] detector in the USA and the AGASA[7] detector in Japan have brought many advances in the understanding of the range of energies between 10^{18} eV and 10^{20} eV, but at a tickling rate. In order to identify the nature of these particles, their origin and mode of production a larger detector is needed if one is to tackle the mysteries associated to them in the foreseeable future.

The Pierre Auger Observatory [17], designed to investigate the UHE cosmic rays with energies beyond $10^{18.5}$ eV over the whole sky, is located in two sites, one in the Southern Hemisphere, in the Mendoza Province, in Argentina, and the other in the Northern, in

*shellard@lafex.cbpf.br
†johana@lafex.cbpf.br
‡amaral@if.uff.br

the state of Utah, in the USA. Each observatory consists of a combination of a ground array, with 1600 Cherenkov detectors, together with four fluorescence detectors aimed at the atmosphere above the ground array. The water tank, which detects the Cherenkov radiation produced by the shower particles crossing it, takes a snapshot of the shower as it hits the ground, while the fluorescence detector measure the longitudinal content of electromagnetic particles within the shower, making a much more precise measurement of its energy. However, the ground array has a full duty cycle, operating all the time, while the fluorescence detector can only work on clear moonless nights, about 10% of the time. The combination of the ground array technique with that of the fluorescence provides a complementary and much more reliable energy and direction measurements, as well the primary component identification[8].

We discuss in this paper the performance of a fluorescence detector which mimics the characteristics of the one planned to be installed in the Southern Hemisphere Pierre Auger Observatory. We simulate its behavior as a function of the air showers energies and triggering conditions. The simulation program used to perform this analysis, FDSIM, was developed by ourselves [18]. We discuss in section 2 the general characteristics of extensive air showers, which are fed in to FDSIM and the fluorescence technique used to detect them. We include, also, a discussion on the atmosphere attenuation effects that dampen the fluorescence signal, and present the expression for the signal detected by the photo multipliers (PMT) at the fluorescence telescopes. We present and discuss the results of the simulation in section 3, leaving our conclusions to section 4.

II EAS and fluorescence detectors

The spectrum of highly energetic cosmic rays falls with a power law, at energies beyond 10^{16} eV, and this flux can be represented by the relation

$$\mathrm{j(E)} = 2.1 \times 10^{7}\ \mathrm{E}^{-3.08}\ \mathrm{m}^{-2}\mathrm{s}^{-1}\mathrm{sr}^{-1}\mathrm{GeV}^{-1},$$

where the energy E is measured in GeV. The flux for energies greater than 10^{19} eV (10 EeV) is not known accurately and is the subject of the measurements of the Pierre Auger Observatory (PAO). Their very low fluxes (one event per km^2 per century above 100 EeV) calls for a large area exposure, 3000 km^2 of a ground array per site at the PAO and the coverage of the atmosphere above this array by the fluorescence telescopes. The air shower is a cascade of particles produced by the interaction of a highly energetic primary cosmic ray with atoms high in the atmosphere. At each collision in the cascade more secondary particles are produced, most of them pions and a few nucleons. The hadronic component of a shower is concentrated very near the axis and difficult to be studied at high energies. The decay of the neutral pions give rise to the electromagnetic cascade which carries $\approx 30\%$ of the primary particle energy and which dissipates approximately 90% of this energy in the process of ionization, while it develops through the atmosphere.

The EAS is characterized by its transversal and longitudinal developments. The quantities associated to the transversal development of the shower, as the particle density, which is a function of the distance to the shower core, or the lateral distribution of the muons, which are generated by pions and kaons decays, can all be measured experimentally in a direct form in a ground array.

To study the longitudinal development of an EAS one may measure the fluorescence of the molecules in the atmosphere associated with the passage of charged particles. The particles in the shower ionize and excite the 2P band of molecular nitrogen and the 1N band of the N_2^+ molecular ion in the atmosphere, which then emit fluorescence photons, typically 10 to 50 nanoseconds after excitation, yielding in average 4-5 photons per electron per meter. Approximately, 80% of the fluorescent light is emitted in the range that varies from 300 to 450 nm, which happens to be a wavelength band for which the atmosphere is quite transparent [10][11]. This fluorescent light is seen by a distant telescope with an optical detector, as a light source moving along the shower axis. The intensity of the light is directly proportional to the number of charged particles at each point of the longitudinal development of the EAS,

$$\frac{dN_\gamma}{dl} = N_f\ N_e, \tag{1}$$

where N_f is the fluorescence yield (typically about 4 photons per charged particle per meter), which is approximately constant in time[11] and N_e, the number of secondary particles produced in the EAS. The integral under this intensity curve is a measure of the energy dissipated in the atmosphere, taking into account the missing energy which evaporates as neutrinos or muons.

The fluorescent light production by the nitrogen molecule in the atmosphere has very low efficiency, which is more than compensated by the huge number of secondary electromagnetic particles in the shower. The number of secondary particles produced in an EAS as a function of its slant matter depth, χ, can be extracted from the Gaisser-Hillas [13] parametrization of the longitudinal shower development, given by:

$$N_e(\chi) = N_{\max}\left(\frac{\chi-\chi_0}{\chi_{\max}-\chi_0}\right)^{\frac{(\chi_{\max}-\chi_0)}{\lambda}} \exp\left(\frac{(\chi_{\max}-\chi)}{\lambda}\right) \quad (2)$$

where $\chi_{\max}$ is the slant matter depth of the maximum of the shower development, χ_0, of the initial point of the shower, all in units of g/cm^2, $\lambda = 70$ g/cm^2 is the mean free path for a proton primary particle, and $N_{\max}$ the shower size at the maximum development. As the EAS moves through the atmosphere, it can be seen by a fixed detector as a fast moving point, producing ultraviolet light, describing a straight path in the night-sky background of starlight, atmospheric glow and man made pollution. As the shower progress, a certain number of PMT's in the detector can be triggered and the shower-detector plane is defined.

Atmospheric showers generate, in addition to fluorescent light, high amounts of Cherenkov light, which is primarily beamed in the forward direction[15]. Cherenkov light in contrast to fluorescent light is not proportional to the total number of charged particles in a shower and has to be filtered out when measuring the energy of the shower. The direct Cherenkov light plays an important role at earlier stages of the shower development, being stronger than the fluorescent light at small emission angles ($\alpha < 20°$). At low altitudes, scattered Cherenkov light may compete with the fluorescent light.

Light traveling through the atmosphere is attenuated either by absorption or by scattering by molecules and aerosols. Absorptive processes are important in the regions of wavelength below 290nm and above 800 nm. Between these range of wavelengths, the main mechanism of attenuation are scattering by the atmosphere molecules (Rayleigh scattering) and scattering by natural or man-made aerosols (Mie scattering[12])[19]. The Rayleigh scattering cross-section has a strong wavelength dependence, ($d\sigma/d\Omega \simeq \lambda^{-4}$), is a stable phenomenon, which depends on the atmosphere density profile, which can be simulated. The number of photons scattered out of a beam, per unit of length is given by,

$$\frac{dN_\gamma}{dl} = -\frac{\rho N_\gamma}{X_R}\left(\frac{400\text{nm}}{\lambda}\right)^4 \quad (3)$$

where $X_R = 2970$ g/cm^2 is the mean free path for Rayleigh scattering at $\lambda = 400$ nm. Mie Scattering, on the other hand, is a highly variable phenomena, which depends on the particulate size and composition, on its distribution and on the vertical density profile. The distribution of aerosols in the atmosphere may change by orders of magnitude over very short spaces of time (normally associated with a weather event), while at other times it can be extremely stable[20]. As a consequence of these considerations, it is more difficult to simulate the Mie scattering and a rigorous study of the characterization of the aerosol content of the atmosphere in the vicinity of the Pampa Amarilla site together with a continuous monitoring of the atmosphere at the site must be certainly performed. For places like deserts and high mountains, where the presence of aerosol is low, we can use a simple model proposed by Elterman et al.[14], where it is assumed that the Mie scattering falls exponentially with the height h. An approximate expression for Mie attenuation near wavelengths of $\lambda = 400$ nm is given by,

$$\frac{dN_\gamma}{dl} \simeq \frac{N_\gamma \ \exp\ (-h \ / \ h_M \ )}{l_M} \quad (4)$$

where h_M is the aerosol scale height (typically ≈ 1.2 km) and l_M, the mean free path, is ≈ 14 km (in the case of the HiRes experiment, for example, the most important effect of the aerosol variability is the change in the factor l_M and three different aerosol models are being considered in order to see which one of them is the most suitable for Dugway[21][22][23][24]).

The attenuation A_{tt} of light passing from a point os slant depth χ_1 and a height h_1 to a point at slant depth χ_2 and a height h_2 due to Mie and Rayleight scattering can be written as,

$$T_{ray} = \exp\left[-\frac{|\chi_1 - \ \chi_2|}{X_R}\ \left(\frac{400}{\lambda}\right)^4\right] \quad (5)$$

$$T_{mie} = \ \exp\left\{\frac{-h_M}{l_M\ \cos\theta}\left(\exp\left(\frac{h_1}{h_M}\right) - \left(\frac{h_2}{h_M}\right)\right)\right\} \quad (6)$$

and $A_{tt} = T_{ray} * T_{mie}$, where θ is the angle in relation to the beam of light. The sensitivity of a fluorescence detector to variations on atmospheric conditions and to the light background allow it to be operated properly only on clear and cloudless nights.

An EAS is seen, from the point of view of a detector, as a fluorescent light spot moving through the night sky background, describing a straight path. The angular motion of the light spot depends on the distance and the orientation of the shower axis. As this light spot moves along the shower axis it emits light isotropically and may be detected by optical sensors whose field-of-view solid angles intersect the shower line.

The signal S detected by the optical sensor depends on the number of electrons in the EAS that are in its field of view, the distance from the shower light spot to the detector, the time over which light is collected by the sensor, the effective area of the telescope and more specifics characteristics of the sensor, like its efficiency. A typical sensor is a Fly's Eye configuration, that is, the detector is formed by a spherical mirror, with a bank of photo multipliers near its focal surface, each of them projecting a solid angle in the sky, defining a sensitivity region. The expression which gives the signal detected by a PMT can be written as[15],

$$S = \frac{A_{Mirr}\ N_e\ Q}{4\pi r^2}\ N_f\ cT\ A_{tt} \tag{7}$$

where N_e is the number of electrons in a piece of the shower of length cT, A_{tt} is the light attenuation factor (caused mainly by scattering), N_f is the fluorescence yield (~ 4.8 photons per electron per meter), Q is the PMT quantum efficiency and r is the distance from the light spot in the shower, to the PMT.

The background noise $\mathcal{N}$ is generated primarily by DC current fluctuations in the PMT's, caused by light from stars, planets and asteroids or from pollution by light coming from urban centers. It is given by[15],

$$\mathcal{N} = \sqrt{4A_{mirr}QBT\delta\Omega} \tag{8}$$

where B is the night sky starlight background and $\delta\Omega$, the pixel solid angle seen by a single PMT. The factor of 4 is used to account for an effective increase in starlight background due to long term air glow and low energy cosmic rays[15]. Consequently, the signal to noise relation is given by,

$$S/\mathcal{N} = \frac{N_e N_f c A_{tt}}{4\pi r^2}\sqrt{\frac{A_{mirr}QT}{4\ \Delta\Omega}}. \tag{9}$$

III Simulation of the behavior of an air shower fluorescence detector

We have developed a simulation program which reproduces the behavior of the fluorescence light generated by an EAS as it crosses the atmosphere and that of the detector. The results presented in this section were obtained using the FDSIM simulation code for the PAO fluorescence detector[18]. One of the main characteristics of this code is that it is written in a very flexible way and, as a consequence, different configuration sites as well as different mirror and PMT specifications can be easily taken into account with only a slight modification in the input data file. Another advantage of this code is that its structure is written in such a way that the addition of new subroutines can be performed in a painless way, without the necessity of great code modifications.

The detector whose behavior we will simulate here is structured by four different eyes, each sitting in a different geographical location. Each eye is made of many telescopes covering a field of view of either 360^0 or 180^0. Each telescope projects a solid angle into the sky with a azimuthal width of 30^0 and an elevation of $28{,}5^0$ (from $2{,}5^0$ in relation to the horizon, up to 31^0). We have used in our analysis the layout of the Pampa Amarilla site[18], in the province of Mendoza, Argentina, where the first of the two Pierre Auger Observatories will be built. The area of coverage by this detector is defined by a six sided polygonal figure, where three of the eyes sit in the periphery, each with an angular coverage of 180^0. At the center of this polygon sits an eye with an angular coverage of 360^0. We show in table 1a the geographical position of each eye and in table 1b the position of the vertices defining the boundary of the array.

Table 1: a) The geographical position of the eyes and their azimuthal coverage; b) The position of the boundaries of the array

Eye	x(km)	y(km)	width
Central	24.00	23.00	360^0
Los Leones	12.36	-3.71	180^0
Los Morados	53.20	18.22	180^0
Positos	20.00	48.53	180^0

	x(km)	y(km)
ArrayPt1	0.43	2.69
ArrayPt2	33.30	-14.62
ArrayPt3	52.00	-6.30
ArrayPt4	55.60	45.20
ArrayPt5	40.00	56.20
ArrayPt6	0.80	42.00

We have simulated 5 000 showers for each of 16 different values of energies ranging from 10^{18} eV to $10^{21.75}$ eV, each set multiplied by a factor of $10^{0.25}$. The showers land on a random point inside a circle of radius 40 km around the central eye. This area is larger than that covered by the ground array, so that one may analyze the fate of shower falling outside the region covered by ground detectors. The showers are generated with a random zenithal angle, obeying a distribution proportional to $\cos\theta^N * \sin\theta$, with N = 2, from 0° to 60°. The projection of the shower into the horizontal plane forms an angle with the west-east line ranging from 0° to 360°, distributed uniformly. The height of the first interaction of the cosmic ray, χ_0, expressed in units of g/cm^2 is generated randomly, according to its mean free path.

In this simulation we have ignored showers that fall within less than 1.0 km from an eye. This is due to the masking of an event in this class, by the Cherenkov light close to the shower core line. We generate an artificial background which reproduces conditions in real life. It has a constant value, but the photo-electrons from this background are generated according to a Poisson distribution. We collect the data only when the signal is three standards deviation from this background. Furthermore we require at least three pixels to be excited to collect the signal from an eye.

We show in figure 1a the fraction of showers falling over the Pampa Amarilla ground array area that are detected by at least one eye, as a function of energy, when the number of excited (triggered) pixels, N_{min}, takes values between 3 and 6. Here and in the next 4 figures, we will show the data obtained using the values N_{min} equal to 3 and to 6. The data for N_{min} equal to 4 and 5 are found to interpolate smoothly between the values 3 and 6. The lines crossing the points in the graph are obtained by requiring a best fit to the points in the plot, and are set to guide the eye of the reader. We observe that for energies higher than about 10^{20} eV there is, practically, no difference between the data obtained with the two triggering conditions, while for energies between 10^{18} eV and 10^{20} eV this difference is less than 7%. For energies higher than 10^{19} eV, independently of the triggering condition used, efficiencies are already higher than 90%, while for energies between 10^{18} eV and 10^{19} eV efficiencies grow very fast, ranging from 48% to 87%, when the more strict triggering condition (N_{min}=6) was used. We must note here that the PAO detectors follow the hybrid concept and we will also have results coming from the ground array stations and from what we can infer from the result of our simulations we expect that we will be able to perform a reliable hybrid reconstruction already for energies greater than 10^{19} eV (with an FD efficiency greater than 90%). We present in figure 1b the impact points in the ground array of showers with energy $10^{18.50}$ eV, which were triggered by the requirement of 6 activated pixels. Here, we can observe that as the energy is low, there are regions that are blind to the FD array, since only showers that fall near the eye are detected. As shower energies are raised, the impact points in the ground array of the detected showers tend to be distributed in a more homogeneous way and for energies greater or equal than 10^{19} eV there is no blind region anymore.

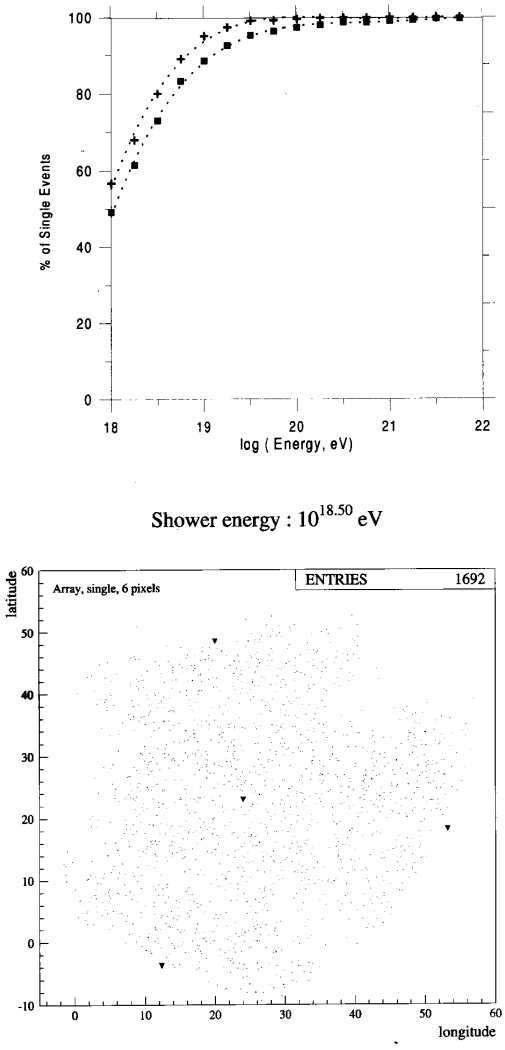

Figure 1. a) Percentage of events falling over the array area that are seen by at least one eye, as a function of the energy, when N_{min} = 3 (+) and 6 (■). The lines crossing the points are obtained by a best fitting and are used from here on as a guide to the reader eyes. b) Snapshot of the array area. The dots represent the triggered events that fall over the array area when $N_{\min}$ = 6 and the triangles give the localization of each one of the eyes.

We present in figure 2a the behavior of the fraction of stereo events falling over the array area (events that are seen simultaneously by two or more eyes) as a function of the shower energy for $N_{\min}$ equal to 3 and 6. Here, we can observe that the differences between data taken using the two triggering conditions are more visible, mainly in the region ranging from $10^{18.75}$ eV to $10^{20.5}$ eV where the two curves can differ by $\sim$ 13%.

While efficiencies are less than 60% for energies less than $10^{18.75}$ eV, independently of the triggering condition imposed, they are higher than 90% for energies equal or higher than 10^{20} eV, allowing us to efficiently reconstruct events in a stereo way for those energies (hybrid reconstruction). We show in figure 2b a snapshot of the array area and the points where these showers are falling over when we, again, use the more strict triggering condition and the primary energy is $10^{18.50}$ eV. We can easily observe from the analysis of this figure that as the energy is very low, events must be near at least to two eyes to be detected, and, as a consequence, there are only three regions, each one of them related to the central eye and one of the peripherical eyes, in which stereo events are detected. Again, as the shower energies are raised, the impact points in the ground array of the detected showers tend to be homogeneously distributed over the whole array area, as expected.

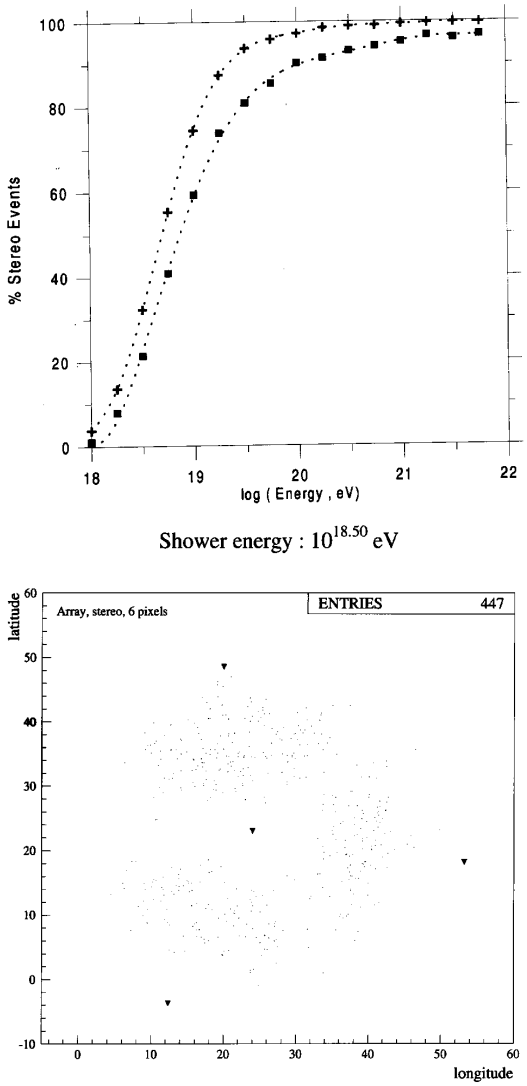

Figure 2. a) Percentage of stereo events falling over the array area, as a function of the shower energy when N_{min}= 3 and 6, respectively (+ and ■). b) Snapshot of the array area. The dots represent the triggered events that fall over the array area when $N_{\min} = 6$ and the triangles give the localization of each one of the eyes.

We have made a study of the contribution of each eye to the overall efficiency and how this efficiency is affected if the central eye is not included in the simulation. We show in figure 3 the behavior of the fraction of events detected by at least one of the three satellite eyes, falling inside the array area, as a function of the shower energy. Here the separation between the trigger requirement of 3 and 6 eyes activated is more pronounced, in contrast to the plot in figure 1a. It can also be seen that for energy values $\geq 10^{19.5}$ eV the efficiencies are already greater than 90%, even when more strict triggering condition is imposed. The Pampa Amarilla FD efficiency when the central eye is not taken into account and when a stereo triggering condition is imposed is shown in figure 4. Here the presence of a central eye is pivotal, for the behavior is very different from the one shown in the figure 2a. The triggering requirements of 3 and 6 pixels show as well a striking difference, more so at the higher energies. The efficiency, when the requirement of at least 6 eyes activated, without the central eye, is less than 80% even at the highest energies which we have simulated the showers, which should be contrasted to the behavior exhibited on figure 2a. The conclusion here is that we may have other array configurations that have equal or even higher performances, but whatever the chosen site layout may be, a central eye is a key ingredient to view EHE cosmic rays in a stereo mode for the same fixed number of eyes.

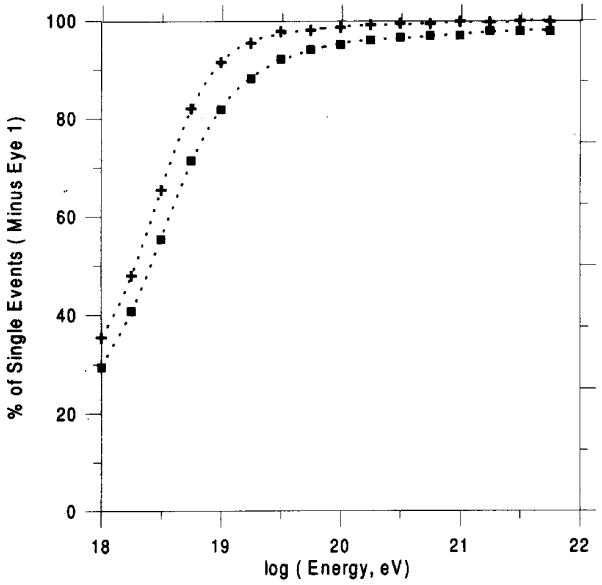

Figure 3. Percentage of events falling over the array area when the central eye is not taken into account, as a function of the shower energy when N_{min} = 3 and 6, respectively (+ and ■).

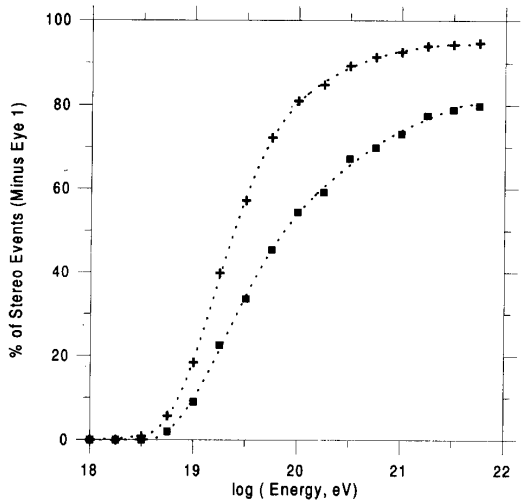

Figure 4. Percentage of stereo events falling over the array area when the central eye is not taken into account, as a function of the shower energy when N_{min}= 3 and 6, respectively (+ and ■).

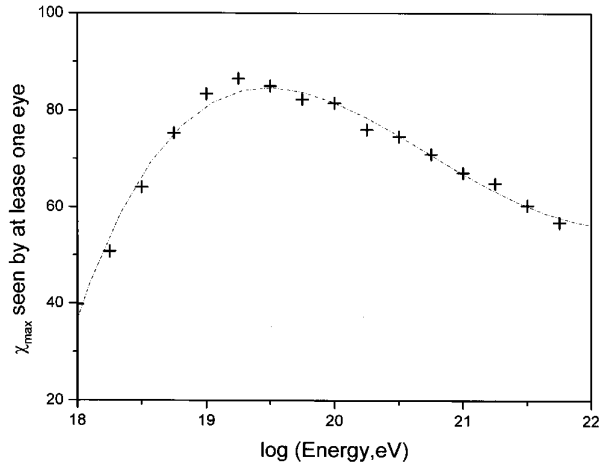

Figure 5. Percentage of events falling over the array area in which the shower maximum is seen by at least one eye when N_{min}=3.

The measurement of the shower maximum is quite crucial for a good determination of the shower energy. We show in figure 5 the behavior of the fraction of events for which the shower maximum is measured by at least one eye, with the requirement that at least 3 pixels are activated. For energies around 10^{18} eV, approximately 39% of the detected events have their maximum point seen by at least one eye (this number should be compared to that of figure 1a). What happens here is that while most of the detected events have their shower maximum point located high above the ground level, some few showers have their maximum point below this level. As the energy is raised, the point where the shower attains its maximum begins to be lowered, and the fraction of events where this point is seen by at least one eye increases up to energies around $10^{19.25}$ eV. After this point, the number of events where the shower maximum point is below the ground level begins to increase as the energy is increased, and, as a consequence the fraction of detected events where the maximum point is seen by one or more eyes decreases and for events with energies greater than 10^{21} the measured efficiencies are already lower than 70%. Actually, we have simulated all the showers with a zenithal distribution which is closer to vertical than in real life, which means that there the efficiency would be a little bit better.

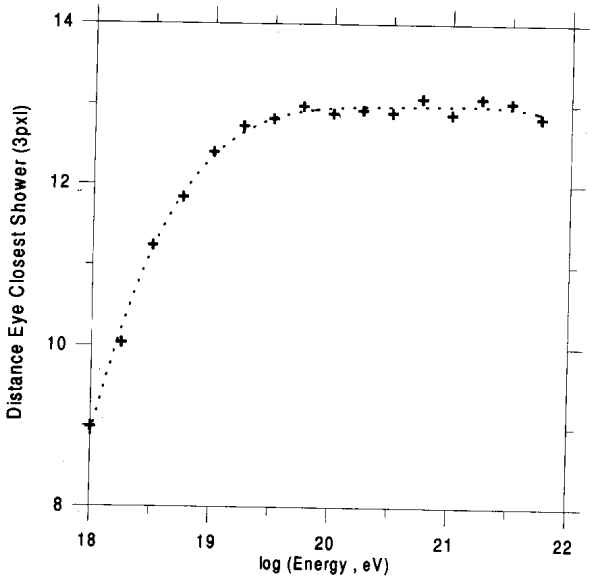

Figure 6. Average distance (in km) between the shower and the closest eye of the events falling over the array area when N_{min}=3.

The average distance (in km) between the shower impact parameter and the closest eye which can trigger, with the requirement of 3 pixels, is presented in the figure 6. The dependence in energy is quite pronounced up to energies of $\approx 10^{19.25}$ eV, when it saturates with the average value of 13 km.

The way how the average number of pixels that are triggered in the eye closest to the shower varies as a function of the shower energies when N_{min} = 3 is shown in figure 7. We observe from the analysis of this figure that, as expected, this number grows as the energy is raised. However, this is figure is a little bit misleading since when we inspect the results of the histograms, for a specific shower energy, from where the data used in figure 7 was taken, we verify it exhibits a strong peak when the number of pixels is equal to 22. This kind of behavior is present for all values of the energies we have studied. As most of the events cross a mirror from the upper part towards the lower one, they typically trigger 22 PMT's.

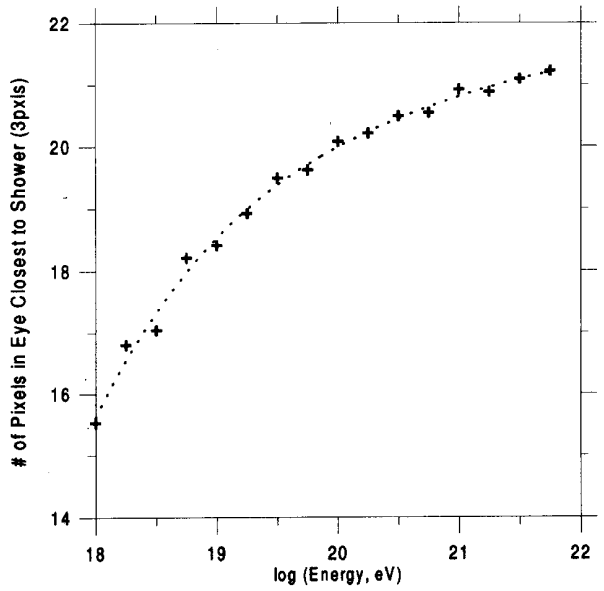

Figure 7. Average number of pixels that are triggered for events falling over the array area, as a function of the energy when N_{min}=3.

The dependence of the behavior of the average angle track-length (in degrees) seen by the closest eye upon the shower energy when $N_{\min}$ =3 is presented in figure 8. From this picture, we observe that, within the range of energies studied, the average angle is quite insensitive to energy variations, since it changes from 22.8° in the lowest energy simulated to $\approx$ 27.5° in the case of the largest energies. However, again, we must note that this result may be a little bit misleading since there is a large peak in all the histograms, for each shower energy, from where the data used in figure 8 were taken. This peak is always located around 30° , and this fact is related to the elevation coverage of the mirrors.

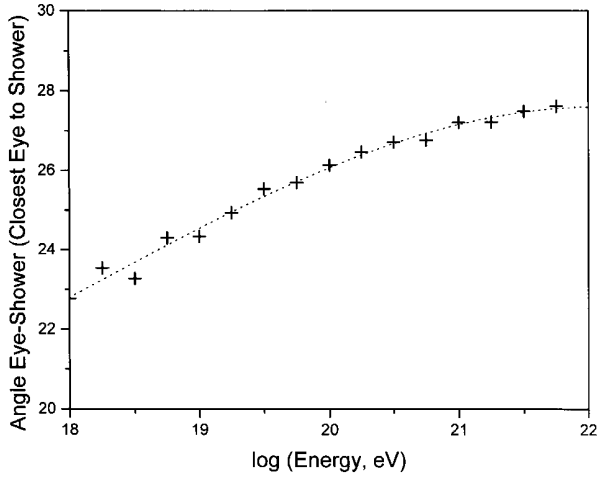

Figure 8. Average track length (in degrees) as a function of the shower energy when N_{min} = 3.

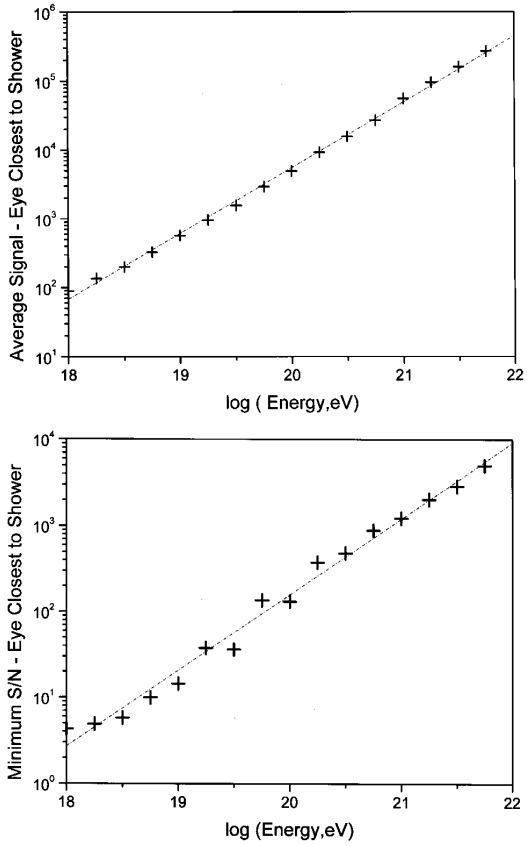

Figure 9. a) Behavior of the average signal (number of photoelectrons) seen by the closest eye when N_{min}=3. b) Average value of the minimum signal to noise detected by the eye closest to the shower as a function of the energy and when the same triggering conditions imposed in figure 9a are met.

We show in figure 9a the behavior of the average signal (number of photoelectrons) seen by the closest eye to the shower, as a function of the energy when $N_{\min}$ = 3, while in figure 9b we show the minimum signal to noise detected by the eye closest to the shower when the shower energy is varied and the same triggering conditions of figure 9a are imposed. Both quantities grow quite considerably as the shower energy grows. The first quantity is much more stable than the second one, although one may not forget that it is a mean quantity. Anyway, what is important is that in the range of energies we are interested in we have a quite good signal to noise relationship.

In figure 10 we show how the average maximum time (in ms) that an event is detected by the closest eye to the shower varies as the shower energies increase. Again we consider here the same triggering conditions used in the last figures. As it was expected for lower energies this average time is lower and as the energy is increased, the average time gets larger until it practically saturates for energies higher than $10^{19.5}$ eV.

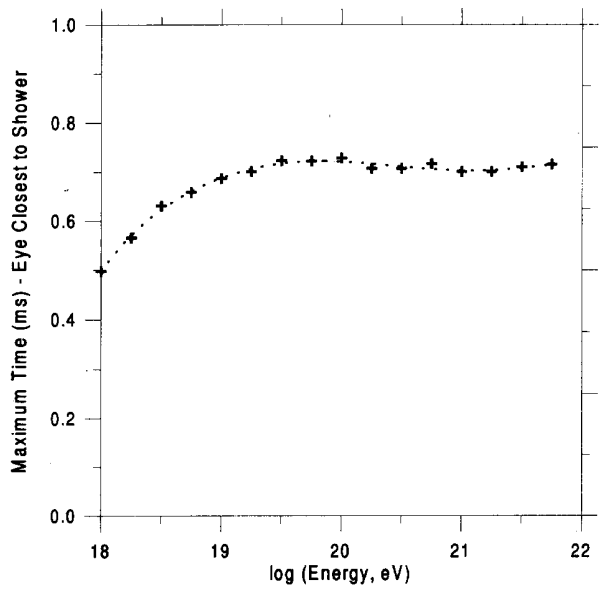

Figure 10. Average maximum time (in milliseconds) that an event is detected by the eye closest to the shower when N_{min}=3.

We have also calculated the fraction of events which are detected outside the ground array area by the central eye only, under the requirement of 3 and 6 eyes activated . In this study we have included showers which fall inside a radius of 40 km around the barycenter of the fluorescence eyes. It is obvious that this result is highly dependent on the value of the circle radius and that our results are only valid for this specific radius value. What is important to note here is that we have verified that events that fall outside the array area, or that pass over the array area without falling inside it, are still detected with efficiencies higher than 80% if their energies are higher than 10^{20} eV, even when we use N_{min} =6. If we relax these triggering conditions and we include the other three satellite eyes we may even detect stereo events outside the ground array area with higher efficiencies. The reason why we may be interested in the efficiency of the detection of showers that may pass over the ground array area without hitting it comes from the fact that since neutrinos are low interacting particles that can induce showers in any part of the atmosphere with equal probability, one way of discriminating them from the other particles is to take into account only showers with zenithal angles greater than 60° (horizontal and quasi horizontal showers are a signature of ultra high energy neutrinos). The fact that, using only the central eye, we are still able to detect events that pass over the ground array area with high efficiencies, is an indication that we may eventually be able to use the PAO Fluorescence detectors to detect neutrino induced showers.

IV Conclusions:

We have made a careful study of the performance of the PAO Fluorescence Detectors in the Pampa Amarilla site. Using our FDSIM code we have simulated, for several different values of the shower energies, the efficiencies of the fluorescence detectors when different triggering conditions are imposed both for single and stereo detection. We have observed that for energies higher than $10^{19.5}$ eV we have obtained efficiencies higher than 80% for all triggering conditions imposed either in single or in stereo detection. If we consider only single detection , taking into account the fact that we will also have results coming from the ground array detectors, we obtain efficiencies higher than 90% for energies greater than 10^{19} eV even when we consider the more strict triggering conditions while in the case of stereo events we will be able to perform an efficient and reliable FD stereo reconstruction for energies greater than 10^{20} eV. We have, also, studied the efficiency of Pampa Amarilla fluorescence detectors (both for at least one eye and stereo detection) when the central eye is not taken into account and have verified that the presence of the central eye is fundamental if we want to have stereo events detected in the desired range of shower energies.

We have shown that the fraction of detected events in which the shower maximum is seen by an eye has a maximum for energies around 10^{19} eV and this result tells us that , for larger values of the energy, we will not be able to determine the position of the shower maximum since it will be located below the ground level We have also investigated the behavior of several important quantities like the track length (in degrees), the average number of triggered pixels, the average maximum time seen by a pixel , the average signal and the minimum signal to noise relationship among others. All these results are consistent one with the others and are a clear indication that, with the fluorescence detectors in the Pampa Amarilla site we will be able to simulate the air showers in a reliable way .We have also verified that it is possible to detect showers outside the ground array area using only the central eye, at least for a circular area with a 40km radius. This fact is interesting if we want to study the possibility of detecting neutrinos with the fluorescence detectors of the PAO, since a signature of neutrino showers are horizontal and quasi horizontal showers. Anyway, it is obvious that one will only be able to answer this question after a careful study of the efficiency of the PAO fluorescence detectors for these kind of showers as a function of the energy and the area where the showers are detected.

Acknowledgments

We would like to thank B. Dawson and C. O. Escobar for many discussions and comments. Thanks also are due to Danays González for discussions about the simulation program.

References

[1] Auger P. , R. Maze, T. Grivet-Meyer , *C. R. Acad. Sci.*, **206** 1721 (1938).

[2] J. Linsley , *Phys. Rev. Lett.* **10** 146 (1963).

[3] M. M. Winn et al, *J. Phys.* **G12** 653 (1986).

[4] M. A. Lawrence ,R. J. O. Reid and A. A. Watson , *J. Phys.* **G17** 733 (1991).

[5] N. N. Efimov et al, *Astrophysical Aspects of the Most Energetic Cosmic Rays*; ed M. Nagano and F. Takahara (World Scientific, Singapore) p 20 (1991).

[6] D. J. Bird et al, *Astrophysics J.* **424** 491 (1994); D. J. Bird , *Astrophysics J.* **441** 144 (1995).

[7] M. Takeda et al, *Phys. Rev. Lett.* **81** 1163 (1998);M. Nagano et al, *J. Phys.* **G18** 423 (1992); N. Hayashida et al, *Phys. Rev. Lett.* **73** 3491 (1994); S. Yoshida et al, *Astroparticle Phys.* **3** 105 (1995).

[8] P. Sommers , *Astroparticle Physics* **3** 349 (1995).

[9] S. Yoshida and H. Dai , *J.Phys.* **G24** 905 (1988).

[10] G. Davidson and R. O'Neil , *J. Chem. Phys.* **41** 3946 (1964).

[11] F. Kakimoto , E. C. Loh ,M. Nagano ,H. Okuno, M. Teshima and S. Ueno , *Nucl. Instr. Methods* **A372** 527 (1996).

[12] M. Z. Jacobson , *Fundamentals of Atmospheric Modeling* (Cambridge U. P., Cambridge) (1999).

[13] T. K. Gaisser and A. M. Hillas , *Proc. of the 15th International Cosmic Ray Conference* **Plovdiv 8** 353 (1977).

[14] L. Elterman and R. B. Toolin , *Handbook of Geophysics and Space Environments (1965).*

[15] R. M. Baltrusaits ,R. Cady ,G. L. Cassidy,R. Cooper,J. W. Elbert ,P. R. Gerhardy,S. Ko,E. C. Loh , M. Salamon,D. Steck and P. Sokolsky, *Nucl. Instr. Methods*, **A240** 410 (1985).

[16] D. J. Bird et al, *Proc. 23rd International Cosmic Ray Conference*, Calgary **2**, 458 (1993).

[17] Pierre Auger Observatory Design Report http://www-td-auger-fnal.gov:82 (1997); US Proposal http://www-td-auger.fnal.gov:82 (1998).

[18] R. C. Shellard , J. C. Diaz and M. G. Amaral , Gap Note to appear (1999).

[19] K. D. Green, *The Cosmic Ray Spectrum Above 0.3 EeV*, Ph.D. Thesis, University of Utah, (1992).

[20] D. J. Bird et al, *Atmospheric Scattering Studies using the High Resolution Fly's Eye Cosmic Ray Detector,* (1997).

[21] C. R. Wilkinson, *The Application of High Precision Timing in the High Resolution Fly 's Eye Cosmic Ray Detector,* Ph.D Thesis, University of Adelaide, (1998).

[22] G. A. D 'Almeida, *J. Geophysical Research,* **92**, 3017 (1987).

[23] D. R. Longtin, *A Wind Dependent Desert Aerosol Model: Radiative Properties,* Air Force Geophysics Laboratory, AFGL-TR-88-0112, (1988).

[24] S. M. Luo, *Tropospheric Aerosol Study by Fly 's Eye and LIDAR Technique,* Ph.D Thesis, Univeristy of Utah, (1992).